KSME

Springer

Journal of Mechanical Science and Technology 38 (8) 2024

Original Article
DOI 10.1007/s12206-024-0715-7

Keywords:
· Double suction pump
· Multi-objective optimization
· Gaussian process regression
· Genetic algorithm
· Numerical calculation

Correspondence to:
Denghao Wu
wdh@cjlu.edu.cn

Citation:
Song, Y., Wu, D., Gu, Y., Ren, Y., Wu, Z., Mou, J. (2024). Multi-objective optimal design of double-suction centrifugal pump impeller using agent-based models. Journal of Mechanical Science and Technology 38 (8) (2024) 4175~4186. http://doi.org/10.1007/s12206-024-0715-7

Received December 8th, 2023
Revised March 10th, 2024
Accepted March 29th, 2024

† Recommended by Editor Han Seo Ko

Multi-objective optimal design of double-suction centrifugal pump impeller using agent-based models

Yu Song[1], Denghao Wu[1], Yunqing Gu[1], Yun Ren[2], Zhenxing Wu[1] and Jiegang Mou[1]

[1]College of Metrology and Measurement Engineering, China Jiliang University, Hangzhou 310018, China, [2]Zhijiang College, Zhejiang University of Technology, Hangzhou 312030, China

Abstract Double suction centrifugal pumps, which feature large flow and head, are applied in water utility and transportation sectors. The efficiency, sound, and vibration levels are key performance indexes for double suction centrifugal pumps. This study aims to improve the performance of double suction pumps using a multi-objective optimization method. The Latin hypercube sampling (LHS) method is used to randomly generate sample data considering five key geometric parameters of the impeller, and the agent model training samples are generated using numerical computation. Then, the multi-objective optimization design of the impeller, focusing on the head, efficiency, and pressure pulsation energy as the objectives, was carried out by combining the Gaussian process regression (GPR) and non-dominated sorting genetic algorithm II (NSGA-II) algorithms. Results show that the head is increased by 3.91 m, the efficiency is increased by 0.2 %, and the pressure pulsation energy is reduced by 24 % compared with the original model. Meanwhile, the detailed information of energy loss and pressure pulsation in the pump was analyzed to understand the influence of impeller geometry parameters. This study provides a certain reference for the optimized design of double-suction pumps.

1. Introduction

Pumps are important tools in human production and life. Among them, the double suction centrifugal pumps, with core features of large flow, high head, and excellent resistance to cavitation, were applied in the petrochemical, cross-basin water transfer. Impellers, are a double suction pump key flow component, whose geometric parameters directly affect the double suction pump performance and operational stability [1]. Therefore, optimizing the impeller of double-suction pump and improving its performance can effectively promote energy conservation and emission reduction initiatives.

Previously, researchers have used various methods to optimize impellers, correspondingly increasing the performance of centrifugal pumps. Traditional optimization methods were mainly used to modify the geometric parameters of the impeller based on their experience. However, these approaches are unstable and depend on the level of experience of the researchers. The design of experiment (DOE) can drastically reduce the number of trials in impeller optimization studies and is therefore widely used. Si et al. [2] ranked the weights of each parameter of the impeller and guide vane on the performance of the centrifugal pump by matrix analysis. Thus, the optimal solution was selected, increasing the pump efficiency by 7.61 %. Wang et al. [3] used the orthogonal test method to optimize the impeller of the centrifugal pump, established an optimization mathematical model with head, efficiency, shaft power, and net positive suction head (NPSH) as the objective function, and experimentally verified that the head, efficiency, and anti-cavitation performance were significantly improved. Zhou et al. [4] selected five geometrical parameters from the impeller for orthogonal tests and obtained the optimum solution for pump efficiency and head by variance analysis. They found a significant performance improvement and pointed out that the pump performance should be optimized for the impeller and

the volute. Although DOE can effectively improve the performance of centrifugal pumps under low-cost conditions, it still has certain limitations. Moreover, the resulting optimization model cannot easily achieve an optimal solution.

Intelligent algorithms are widely used in various fields because of their excellent performance and versatility. Researchers have begun combining agent models and optimization-seeking algorithms into centrifugal pump optimization design methods. Zhang et al. [5] proposed a kriging model with the objective of optimizing pump efficiency and cavitation margin. They compared the NSGA II and MOEA/D optimization results and found that MOEA/D can effectively obtain the Pareto optimal solution set. Tao et al. [6] used a cavitation-inspired strategy to achieve the required head for the optimized pump design conditions, with a significant improvement in efficiency and anti-cavitation performance. Shahram et al. [7] used the eagle strategy algorithm to divide the optimization process into two phases, roaming and chasing, thereby increasing the head and efficiency of centrifugal pumps. Zhou et al. [8] used the loss extremum method to establish an objective function based on minimum hydraulic loss. Then, they used a genetic algorithm to determine the impeller model with the best efficiency to enhance the performance of double-suction pump. Pei et al. [9] used an optimization method combining particle swarm algorithm and two-layer neural network to improve the efficiency of centrifugal pumps. This approach addresses the correspondence between centrifugal pump performance and optimized variables. Therefore, the intelligent algorithm is suitable for application in the field of centrifugal pump optimization design, greatly reducing the optimization cost and the research time. The optimization effect is stable and less dependent on the experience of researchers.

Most studies on optimization focus on pump performance but ignore pressure pulsation. Pressure pulsation is related to the operational stability and vibration noise level of the pump. To further improve the performance of double-suction pumps, a combination of Gaussian process regression algorithms and genetic algorithms is used to optimize the head, efficiency and pressure pulsation energy of double suction pump. The GPR is used to predict the performance data of double suction pumps under different impeller models, and the genetic algorithm is used to identify the optimized model. Meanwhile, the influence of the impeller geometry parameters on the flow and pressure pulsations was investigated by analyzing the flow characteristics and pressure pulsation distributions within the double-suction pump.

2. Pump model and CFD setup

2.1 Double suction pump model

Fig. 1 shows the main components of a double-suction centrifugal pump. Pump performance data under rated operating condition are as follows: Q_d = 1040 m^3/h, H_d = 75 m, n_d = 1490 r/min, and η_d = 84 %. Table 1 shows the main geometric parameters of the double-suction pump.

Table 1. Main geometric parameters of the double suction pump.

Parameters of impeller	Value
Inlet diameter D_1	236 mm
Outlet diameter D_2	489 mm
Blade thickness e_1	5 mm
Blade inlet angle β_1	20°
Blade outlet angle β_2	22°
Blade wrap angle φ_1	145°
Number of blades Z	7

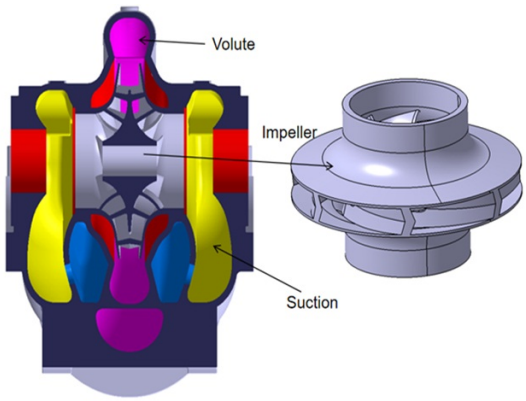

Fig. 1. Schematic of double suction pump structure.

2.2 Numerical calculation method

The computational domain of the double suction pump contains the impeller, suction, volute, chamber, and inlet/outlet extension section, where the length of the extension section is 10 times its diameter to ensure the inlet/outlet flow stability.

To achieve consistent results of the centrifugal pump simulation calculations to the experimental findings, the SST k-ω turbulence model is selected for simulation [10], and the standard root-mean-square (RMS) of convergence is set to 10^{-5}. The impeller is set to rotate and the other areas are set to stationary. A frozen rotor pattern is used on the interaction surfaces of the rotating and stationary regions, e. g., the impeller–volute interaction surface. The inlet condition includes a total pressure inlet where the pressure is set to 0 Pa, and the outlet condition involves a mass flow outlet, which is set according to the demand of the working condition. The wall roughness of the impeller, suction chamber, and volute is set to 0.04 mm to achieve realistic simulation results [11].

The number of meshes affects the numerical calculation results [12]. Insufficient grids lead to inaccurate numerical simulation results, whereas excessive grids require considerable computational resources. Thus, the appropriate number of grids needs to be experimentally selected. In this study, the calculation results under rated operating condition are selected to verify the grid independence (Table 2).

Table 2. Grid-independence verification results.

No.	Number of grids (/10^6)	H(m)	$\Delta H = \lvert H_i - H_5 \rvert / H_5$ (%)	η (%)	$\Delta \eta = \lvert \eta_i - \eta_5 \rvert / \eta_5$(%)	RMS_a	$\Delta RMS_a = \lvert RMS_{ai} - RMS_{a5} \rvert / RMS_{a5}$ (%)
1	7.0	81.40	5.22	84.30	0.45	192.21	4.01
2	7.8	79.00	2.12	84.48	0.22	196.59	1.83
3	9.1	78.39	1.33	84.45	0.26	197.43	1.41
4	10.2	77.84	0.62	84.54	0.15	198.17	1.04
5	12.1	77.36	0	84.67	0	200.25	0

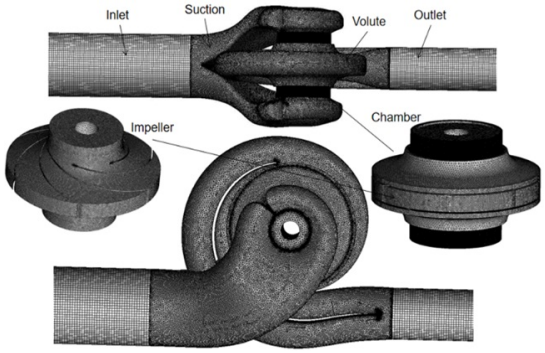

Fig. 2. Fluid domain and mesh of the computational model.

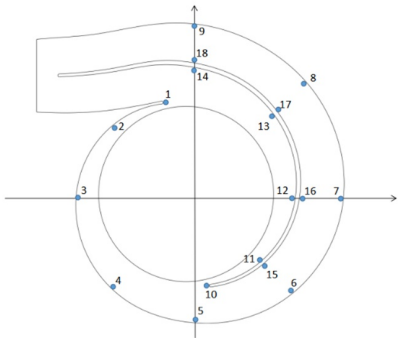

Fig. 3. Pressure pulsation monitoring points.

The errors were compared, and the results showed that the pump performance started to become stable at 9.1 million grids with less time consumed. Thus, the appropriate grid number is 9.1 million.

To analyze the pressure pulsation in the unsteady flow field inside the double suction pump, we arranged 18 monitoring points inside the volute to control the pressure pulsation. The 18 points are located in the middle cross-section of the volute, and the monitoring points are numbered from 1 to 18 (Fig. 3).

2.3 Numerical simulation validation

The simulation data of the original model are compared with the test data to verify the accuracy of the numerical simulation results (Figs. 4 and 5); the test and numerical simulation results are basically consistent.

The average error of the efficiency is 2.22 %, the maximum error is 6.79 %, and the large deviation of the head and efficiency has occurred at high flow rates. The head and efficiency errors of the nominal conditions are less than 2.5 %. Therefore, predicting the pump performance is feasible by numerical simulation instead of test.

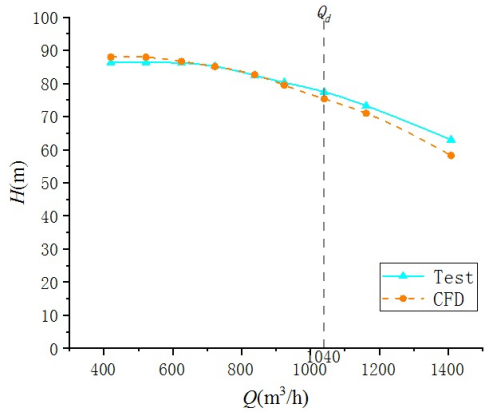

Fig. 4. Numerical simulation and experimental results of head.

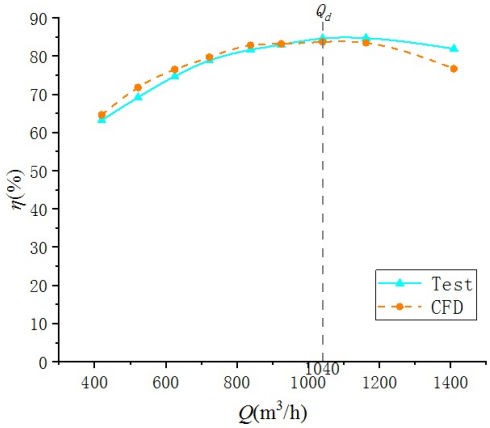

Fig. 5. Numerical simulation and experimental results of efficiency.

3. Optimization processes

3.1 Optimization goals

The optimization objectives involve the head, the efficiency, and RMS_a at rated operating conditions. RMS_a represents the average pressure pulsation energy at each monitoring point at rated operating conditions in the dimensionless unit. The calculation procedure for RMS_a includes the following procedures

[13]:

Step 1: The pressure pulsation factor C_p is calculated, as follows.

$$C_p = \frac{p_i - \overline{p}}{0.5\rho u^2}, \tag{1}$$

where p_i is the instantaneous static pressure value, Pa; $\overline{p}$ is the average static pressure value; ρ is the density of the fluid, kg/m^3; u is the impeller circumferential exit velocity, m/s.

Step 2: Fourier transform is performed to obtain the pressure pulsation spectrum at each measurement point.

Step 3: To express the pressure pulsation energy at the pump measurement point, the pressure pulsation coefficients from 0 Hz to four times the blade passing frequency ($4f_{bpf}$) are processed as root-mean-square, as follows:

$$RMS = \frac{1.63}{2}[\frac{1}{2}(\frac{1}{2}C_{p_0}^2 + \sum_{n=2}^{n-1} C_{p_{n-1}}^2 + \frac{1}{2}C_{pn}^2)]^{0.5}. \tag{2}$$

Step 4: The RMS values at each measurement point are averaged and expressed as RMS_a, and the energy of pressure pulsations in the low-frequency range of the pump is characterized.

$$RMS_a = \frac{1}{N}\sum_{i=1}^{N} RMS_{pi}. \tag{3}$$

3.2 Selection of optimization parameters

The geometrical parameters of the impeller can greatly influence the hydraulic performance of a double suction pump. However, consdiering all the geometrical parameters of the impeller is infeasible during the optimizing processes due to limited computational resources. Therefore, selecting some key parameters as inputs for optimization is necessary. Eleven parameters were initially selected based on previous studies. The impeller outlet diameter changes the parameters of the volute; thus it is not selected in this study. The front and rear plate curves of one of the impeller blades follow a five-point four times Bessel curve. Adjusting the longitudinal coordinates of three points can control the impeller front and rear plate curves given that the first and last control point for the endpoint and the inlet section curve is tangent to the inlet. These parameters were further filtered by the Plackett–Burman experiment [14].

In this paper, we designed a thirteen-factor bilevel Plackett-Burman experiment with 20 trials and a confidence level of 90 %, where two factors (factor M and factor N) as dummy variables are for reference only.

Fig. 7 shows the results of the Plackett–Burman experiment, where the x-axis represents the factor impact coefficients. Variables with factor impact coefficients exceeding the red line are considered significant. Through the analysis, five parameters, b_2, β_1, β_2, φ_1, and Z, with the most significant impact are selected as optimization variables.

Table 3. Range of optimization variables.

No.	Parameters of variables	Value
A	Number of blades Z	[6, 7]
B	Blade inlet angle β_1	[14°, 22°]
C	Blade outlet angle β_2	[16°, 30°]
D	Blade wrap angle φ_1	[120°, 160°]
E	Impeller outlet width b_2	[48, 56]
F	Shroud point P_1	[78, 92]
G	Shroud point P_2	[59.6, 63.6]
H	Shroud point P_3	[46.5, 49.9]
J	Hub point P_1'	[63.6, 74.6]
K	Hub point P_2'	[13, 18]
L	Hub point P_3'	[7.5, 11.9]

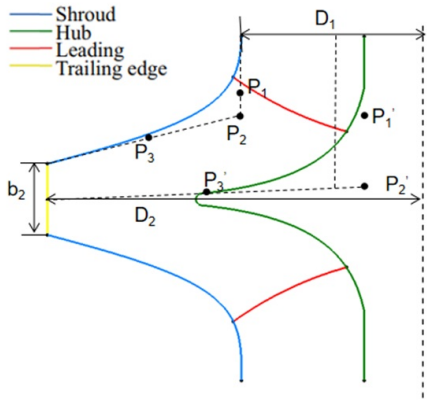

(a) Meridional shape of impeller

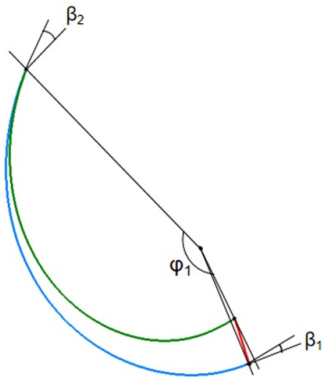

(b) Shape of blades

Fig. 6. Optimization variables.

The fitting of an agent model requires a large amount of sample data for training, and to obtain a better fit, the sampling should cover the entire range of variable values as much as possible. The LHS method [15] is finally adopted in this , given its excellent space-filling ability, to extract variable samples. Moreover, 60 samples are extracted within the optimization range for the five optimization parameters. 3D modeling and

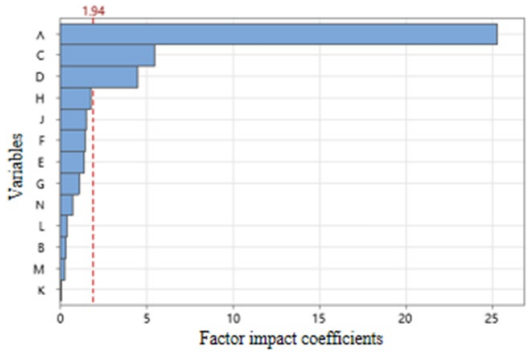

(a) Head

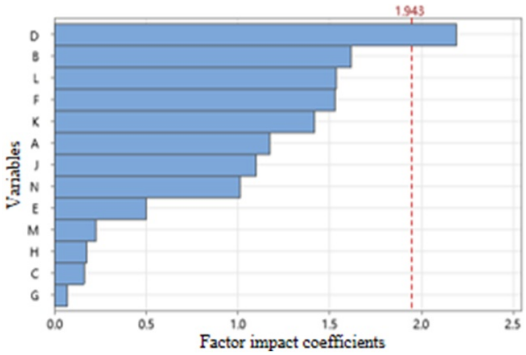

(b) Efficiency

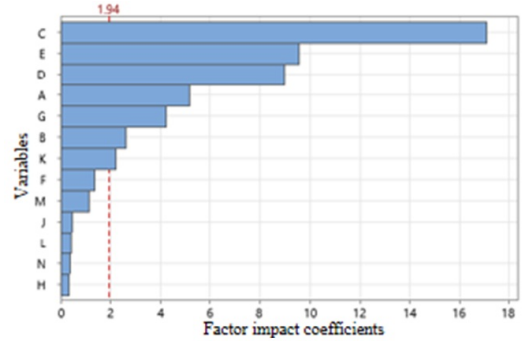

(c) Pressure pulsation

Fig. 7. Pareto equivalence table for the Plackett–Burman experiment.

simulation calculations were performed on these 60 models, and these data were used as the agent model training data.

3.3 Gaussian process regression

A Gaussian process includes a set of random variables in which any finite number of random variables taken together exhibits a joint Gaussian distribution. For ease of understanding, a Gaussian process can be considered a probability distribution of a function whose properties are determined by the mean and covariance functions. Gaussian process regression (GPR) initially builds a prior function based on Bayesian principles. Then, a training dataset is used to transform it into a posterior distribution that can be extrapolated to the hyperparameters of the kernel function. This condition results in the following Gaussian process regression equations [16], where $\overline{f_*}$ is the predicted mean vector.

$$f_* \left| X, y, X_* \sim N(m_*, \mathrm{cov}(f_*)) \right. , \tag{4}$$

$$m_* = E\left[f_* \left| X, y, X_* \right. \right] = K(X_*, X)(K(X, X) + \sigma_n^2 I)^{-1} y , \tag{5}$$

$$\mathrm{cov}(f_*) = K(X_*, X_*) - K(X_*, X)(K(X, X) + \sigma_n^2 I)^{-1} K(X, X_*) . \tag{6}$$

GPR uses Bayesian inference and infinite parameters to determine the relationship between inputs and outputs. GPR is often used for predictive computation in various domains and is well adapted to situations with small amounts of data, high dimensionality, and nonlinearity [17, 18].

This study compares the centrifugal pump performance prediction levels of GPR and artificial neural network (ANN). Evidently, the prediction points of the GPR model for head, efficiency, and RMS_a are more clustered around the theoretical prediction straight line. Therefore, this study adopts the GPR model as the performance prediction model for double-suction centrifugal pumps. The proposed kernel function for Gaussian process regression uses a quadratic rational kernel, and the GPR model was trained using a five-fold cross-validation method.

3.4 Multi-objective optimization

Multi-objective optimization involves optimizing the performance of multiple pumps simultaneously while adhering to various limitations. This condition often leads to conflicts between the objectives; thus, identifying a single optimal solution becomes challenging. Alternatively, the focus should be on selecting the most favorable better solution among these objectives [19]. In this study, the optimization objectives include minimization of RMS_a, maximization of H, and maximization of η. The optimization variables are b_2, β_1, β_2, φ_1, and Z. It is a typical multi-objective optimization problem whose mathematical expression is shown in Eq. (7).

$$\begin{cases} Find & \mathrm{X}=[b_2, \beta_1, \beta_2, \varphi_1, z] \\ \begin{cases} Minimize & RMS_a = f_1(b_2, \beta_1, \beta_2, \varphi_1, z) \\ Maxmize & H = f_2(b_2, \beta_1, \beta_2, \varphi_1, z) \\ Maxmize & \eta = f_3(b_2, \beta_1, \beta_2, \varphi_1, z) \end{cases} \\ Subject\ \mathrm{to} & 48\mathrm{mm} \le b_2 \le 56mm \\ & 14^\circ \le \beta_1 \le 22^\circ \\ & 16^\circ \le \beta_2 \le 30^\circ \\ & 120^\circ \le \varphi_1 \le 160^\circ \\ & 6 \le z \le 7 \end{cases} . \tag{7}$$

The optimal design of a pump requires balancing the conflicts between the optimization objectives, indicating more than one optimal solution. The Pareto method is used to compose

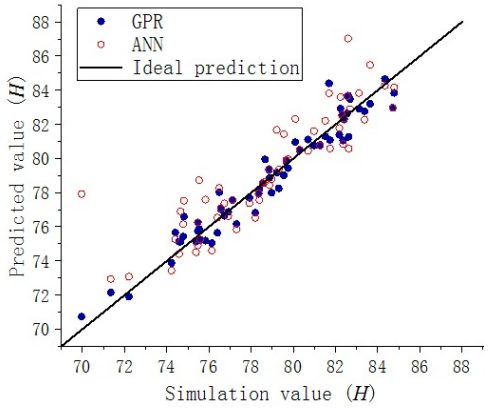

(a) Head

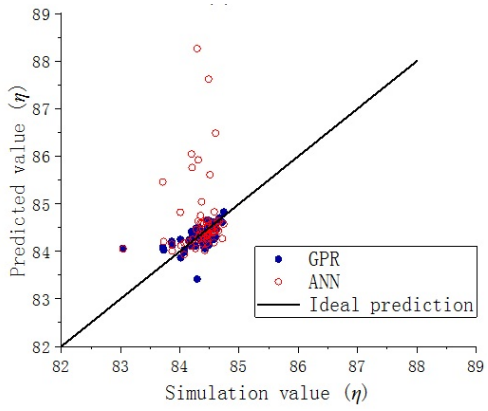

(b) Efficiency

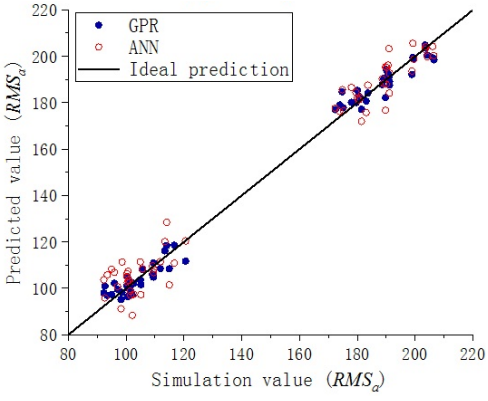

(c) Pressure pulsation

Fig. 8. Comparison plot of ANN and GPR prediction levels.

all non-dominated solutions into a Pareto front, from which the designer is free to select the solution that satisfies the requirements [20].

Genetic algorithms can obtain optimization results faster when solving complex combinatorial optimization problems, and it is currently the most popular optimization algorithm [21, 22]. In this study, non-dominated sorting genetic algorithm II (NSGA-II) was used. It is an improved multi-objective genetic algorithm with enhanced convergence and distribution of the solution [23]. At the core, the non-dominated sorting and elite retention strategies are available. The non-dominated sorting approach balances conflicts between goals, and the elite retention strategy ensures the direction and speed of convergence of the population. NSGA-II was used to perform multi-objective optimization of RMS_a, H, and η, setting the number of populations to 300, the number of iterations to 20000, the crossover probability to 0.9, and the variance probability to 0.1.

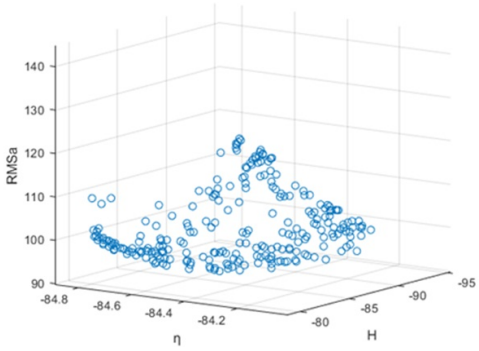

Fig. 9. Pareto front.

4. Results and analysis

4.1 Pareto front

Fig. 9 shows the Pareto front obtained from NSGA-II calculations. The final optimization case needs to be selected from the non-dominated solutions in the Pareto front, which are relative optimal solutions. The two techniques to determine the optimal solution encompass assigning weights to each optimization objective and decision-making processes. In this study, the TOPSIS method, which is a widely used decision-making process method [24, 25], is preferred.

Step 1: The optimization objective is homogenized with dimensionless parameters.

Step 2: The distances of the points on the Pareto front from the ideal and non-ideal points are calculated.

Step 3: The distance values are combined to calculate the composite degree scores and then rank them.

The main optimization objectives include improving efficiency and reducing pressure pulsation. Therefore, in selecting the optimal model, we ensure that H is not lower than the original model H, and the minimization of RMS_a and maximization of η are pursued. The solutions with lower head on the Pareto front than the original model head are removed, and then the optimized solution is selected from the remaining Pareto solutions using the TOPSIS method as the optimized solution A (shown as red circle in Fig. 10). For comparison, the optimal solutions B and C are then selected, where B is η optimal solution and C is the RMS_a optimal solution. CFD numerical simulations of the optimized model were carried out to verify the accuracy of the predictions of the GPR algorithm and to study the flow in the pump.

Table 4 illustrates that the errors of GPR in predicting head are less than 1.2 %, the prediction errors of η are less than

Table 4. Range of optimization variables.

Variables		Original	A	B	C
Z		7	7	7	7
β_1/(deg)		20	18.8	18.7	18.3
β_2/(deg)		25.2	23.6	20	26.8
φ_1/(deg)		145	134.5	135.2	137.8
b_2/(mm)		52.6	50.8	51.8	49.8
GPR	H_d/(m)	78.07	80.47	77.79	82.29
	η/(%)	84.65	84.68	84.76	84.39
	RMS_a	127.76	97.39	107.81	94.59
CFD	H_d/(m)	77.46	81.37	78.39	82.76
	η/(%)	84.59	84.76	84.82	84.48
	RMS_a	131.46	99.89	109.79	96.91
Rel. error	ε_H/(%)	0.65	0.74	0.77	0.57
	ε_η/(%)	0.07	0.09	0.07	0.11
	ε_{RMS}/(%)	2.81	2.50	1.80	2.39

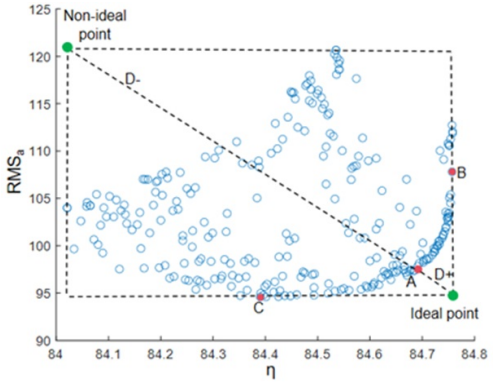

Fig. 10. Pareto solution sets for RMS_a and η.

0.2 %, and those of RMS_a are less than 2.8 %. These findings confirm that GPR is applicable and performs effectively in predicting the performance of pumps.

In details, case A exhibits a head increase of 5.05 %, an efficiency increase of 0.2 %, and a pressure pulsation energy decrease of 24.01 % over the original case. Case B presents a head increase of 1.2 %, an efficiency increase of 0.27 %, and a pressure pulsation energy decrease of 16.48 %. Case C illustrates a head increase of 6.84 %, an efficiency decrease of 0.13 %, and a pressure pulsation energy decrease of 26.28 %. The original model is compared with cases A and B, and the results showed that the efficiency improvement has a certain limitation given the excellent design of the original mode. However, the comparison between cases A and C indicates that increasing the outlet angle and decreasing the outlet width appropriately can increase the head and reduce the pressure pulsation.

Cases A and B outperform the original case, with a large improvement in H and RMS_a. Case C exhibits less η than the original model although H and RMS_a are optimized. Case A is confirmed to satisfy the requirements and is therefore considered the optimal model. The pressure pulsation energy and unsteady flow characteristics are investigated by comparing case A with other cases.

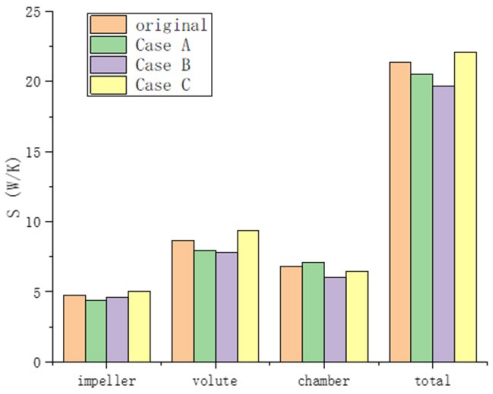

Fig. 11. LEP and TEP of original case and optimize cases at 1.0Q_d.

4.2 Energy loss analysis

The entropy production theory can identify energy losses by locating and quantifying energy losses. Moreover, many studies have applied the entropy production theory to reveal the characteristics of energy losses within the rotating machinery [26-30]. Fig. 11 shows the total entropy production (TEP) and local entropy production (LEP) values of the components of the original case and optimization cases at rated operating conditions. The LEP of scheme A is higher than that of the original model, but the difference is small with only slight effect, and the overall TEP is still reduced. The LEP of the impeller and volute parts of cases A and B are reduced compared with the original case. This law coincides with the CFD calculation of the head and the efficiency increase, further demonstrating the optimization effect of the optimization method.

The energy losses of the double suction pump were determined by analyzing the average entropy production rate (EPR) distribution in each region of the optimization model under design conditions, as shown in Fig. 12. Impeller entropy production distribution is mainly concentrated in the suction side of the blade as well as the exit position of the pressure side surface due to the energy loss arising from the change in the direction and speed of fluid flow into the impeller.

The entropy production distribution is mainly concentrated in the tongue and spacer plate components of the volute, which are close to the position of the impeller outlet, because of the rotor–stator interaction interference between the impeller and volute. In addition, the energy loss caused by the fluid impact on the volute is increased in cases A and C because of the increase in the outlet angle of the impeller. However, the energy loss on the impeller volute interaction surface is greatly improved in case A. Thus, the LEP of the volute is significantly reduced.

Double suction pumps do not always work under design conditions but sometimes operate under non-design conditions

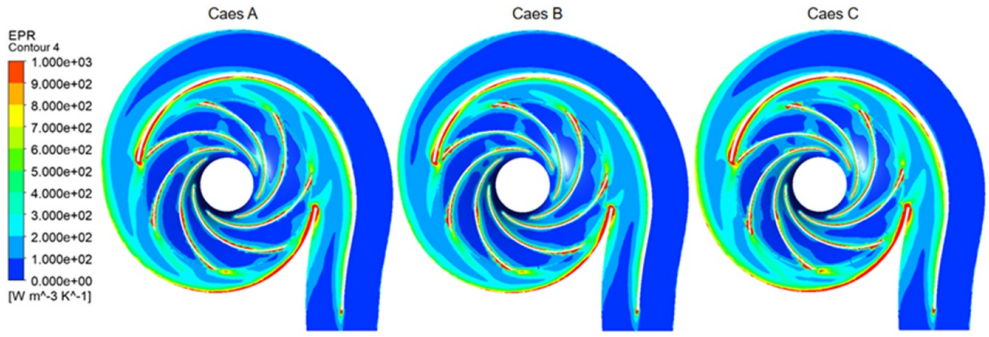

Fig. 12. EPR distribution of optimize cases under 1.0Q_d.

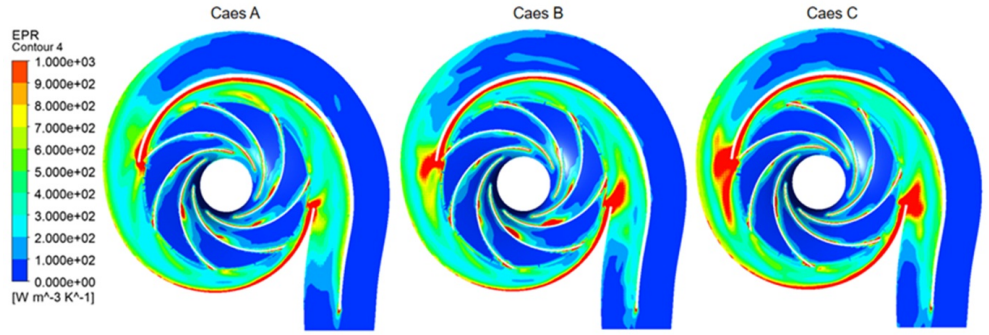

Fig. 13. EPR distribution of optimize cases under 0.8Q_d.

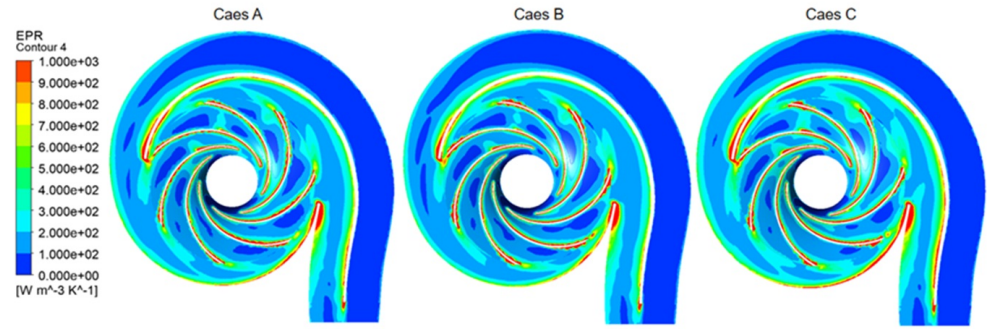

Fig. 14. EPR distribution of optimize cases under 1.2Q_d.

due to changes in the operating environment. Therefore, the optimization of non-design conditions is also greatly important. In case A, the pump head is improved at 0.8Q_d, whereas the efficiency remains more or less the same. However, at 1.2Q_d, the head and efficiency are improved. The energy loss in the pump under non-design conditions is also analyzed to explore on the principle of optimizing the model for performance enhancement. Fig. 13 shows the EPR distribution for optimized cases under 0.8Q_d. At 0.8Q_d, the fluid flow in the impeller is very disordered, resulting in large energy losses in the middle part of the suction side of the blade. The energy loss in the volute tongue and spacer plate portions is substantial at 0.8 Q_d, especially in cases B and C. This finding indicates that the efficiency of case A is better maintained at 0.8 Q_d.

Fig. 14 shows the distribution of the EPR of the impeller and volute at 1.2 Q_d operating conditions. At 1.2 Q_d, the energy loss inside the impeller is very serious; it is mainly concentrated on the suction side of the blades as well as the inlet and outlet positions of the pressure side surface due to the high flow rate. This condition greatly increases the energy loss due to the fluid entering the impeller and impacting the blades. At 0.8 and 1.0 Q_d, the distribution of the entropy production of the volute is mainly concentrated in the tongue and spacer plate sections of the volute, which are close to the impeller and the volute outlet. The energy loss inside the volute is improved at 1.2 Q_d, resulting in a significant reduction in the energy loss of the volute. This condition explains the increase in efficiency of the double suction pump over the original pump at 1.2 Q_d, indicating a further improvement in the flow in the pump at high flow rates. The energy loss in case B is significantly smaller than that in

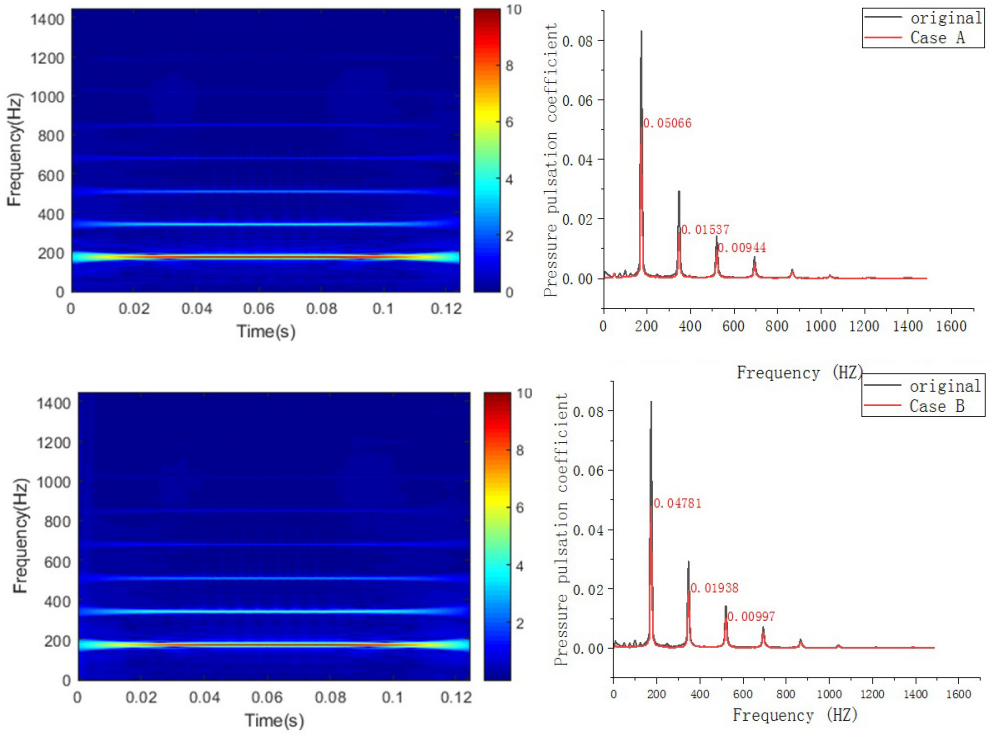

Fig. 15. Time-frequency domain comparison of pressure pulsations at monitoring point 1.

the other cases. This finding verifies that case B is more efficient than the other cases in high flow cases.

4.3 Pressure pulsation analysis

Among the nine monitoring points on the outer surface of the volute, monitoring point 1, is located in the spacer tongue portion of the volute. Moreover, the point, where the rotor–stator interference is the most significant, is selected for analysis for each case. A comparison of the time-frequency domain of pressure pulsations at monitoring point 1 for each case is shown in Fig. 15.

The figure shows that for each case before and after the impeller optimization, the characteristic frequency of each monitoring point is evident, concentrating on the blade passing frequency (f_{BPF} = 173.83 Hz) and its octave. This finding is related to the rotor–stator interaction interference between the impeller and the volute tongue. Furthermore, the pressure pulsation increases with its proximity to the impeller outlet, the pressure pulse amplitude at the monitoring point 1 of the optimized cases decreases evidently in the blade frequency and its octave, and case A has the most significant optimization effect. In addition,, the pressure pulsation characteristic frequency has some low frequencies, exhibiting reduced shaft frequency (f_n = 24.83 Hz) and its octave after optimization. Overall, the pressure pulsation energy is mainly concentrated in the frequency range of 0–4 f_{BPF}, which is consistent with the literature results. The result indicates that RMS_a maintains the root mean square of the pressure pulsation coefficient within 0–4 f_{BPF}, which can characterize the pressure pulsation energy in the low frequency band of the pump. The pressure pulsation energy of case A is slightly higher than that of case B at f_{BPF} due to the increased impeller outlet angle. However, it will be better than that of case A at twice as well as many times the f_{BPF}, which is the reason why case A is better than case B in the RMS_a.

In this study, monitoring point 10 of the nine monitoring points on the volute spacer plate was selected for the main analysis. Monitoring point 10 is the starting position of the volute spacer plate and it is the monitoring point with the largest pressure pulsation on the volute spacer plate. The time-frequency domain comparison of pressure pulsation at monitoring point 10 on the volute spacer plate before and after optimization is shown in Fig. 16.

After the impeller optimization, the amplitude of pressure pulsation at monitoring point 10 of each case decreased, but its optimization effect was not as excellent as that of monitoring point 1. This finding is due to the fact that the high-velocity liquid flowing from the impeller at monitoring point 10 mixes with the liquid in the spiral section of the volute, resulting in large pressure fluctuations. Therefore, pressure fluctuations are still large here after optimization, but pressure pulsation has been improved in relation to that of the initial double suction pump, confirming the success of the impeller optimization. The optimization of monitoring point 10 is consistent with that of monitoring point 1, with case B performing slightly better than the cases A on the f_{BPF}, contrary to case A on the blade frequency octave, resulting in a lower RMS_a than that of case A.

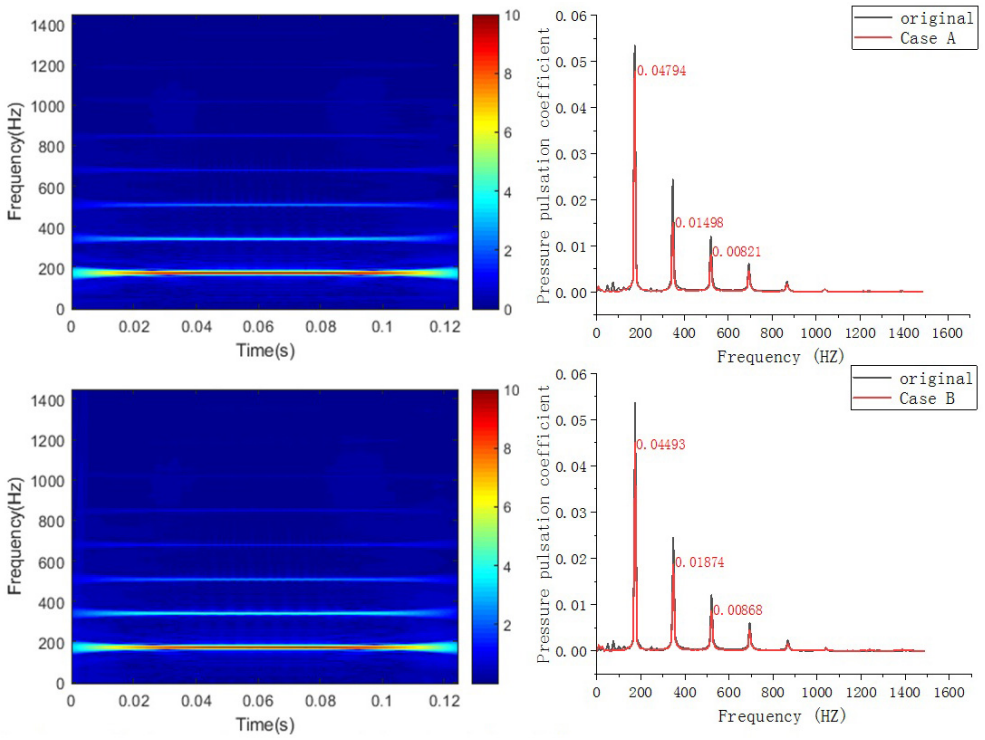

Fig. 16. Time-frequency domain comparison of pressure pulsations at monitoring point 10.

5. Conclusions

A multi-objective optimization method combining GRP and NSGA-II is used to optimize the design of the impeller of a double suction pump. This optimization aims to pursue the maximization of H and η and the minimization of RMS_a under the design conditions. Sixty models were obtained by the LHS method as training models for GRP. A five-input, three-output GPR is employed to fit the mapping function between the optimization variables and the optimization objective, and the comparison of the prediction results with the CFD results verified the prediction accuracy of the GPR. NSGA-II is used to obtain the Pareto front, and the optimal solution was selected by TOPSIS. To investigate the mechanism of optimization model to enhance the pump performance, the energy loss characteristics are assessed based on the entropy production theory, and the pressure pulsation characteristics are analyzed by comparing the pressure pulsation in time and frequency domains. The following conclusions are drawn:

1) The multi-objective optimization method combining GPR and NSGA-II successfully optimized the performance of the centrifugal pump under the design conditions, increasing H of double suction pump by 3.91 m, increasing η by 0.2 %, and reducing RMS_a by 24.01 %.

2) The LEP and TEP of the components of the optimized and original cases were compared, and the results showed that the energy losses in the impeller and volute were improved. The energy loss under non-designed conditions is also analyzed. In the low flow case, the unstable flow causes a large amount of energy loss, mainly at the middle of the suction side of the blades, at the outer surface of the volute, and at the spacer plate. In the high flow case, the energy loss is concentrated on the impeller blade surface and less on the volute.

3) The characteristic frequencies of each monitoring point, concentrated in the blade frequency and its octave, were related to the rotor–stator interaction, they were significantly reduced after optimization, and the low-frequency pulsations were improved. Overall, the pressure pulsation energy is mainly concentrated in 0–4f_{BPF}. The RMS_a can characterize the pressure pulsation energy of the pump in the low-frequency band.

4) The pressure pulsation energy of double-suction centrifugal pumps was comprehensively evaluated using RMS_a as an index by means of multi-objective optimization. This approach successfully reduces the pressure pulsation energy at each measurement point in the pump and provides a guide to the design of pump with low vibration and noise level.

Acknowledgments

This work was supported by the Natural Science Foundation of Zhejiang Province (No. LGG21E090002, LY21E060004), and Zhejiang Province Key Research and Development Program (No. 2021C01052).

Nomenclature

LHS : Latin hypercube sampling

GPR : Gaussian process regression
NSGA-II: Non-dominated sorting genetic algorithm II
MOEA/D: Multiobjective evolutionary algorithm based on decomposition
ANN : Artificial neural network
H : Head
η : Efficiency
RMS_a : Root mean square of pressure pulsation coefficient
Q_d : Flow rate at rated operating condition
H_d : Head at rated operating condition
n_d : Rotation speed at rated operating condition
LEP : Local entropy production
TEP : Total entropy production
f_{BPF} : Blade passing frequency
f_n : Shaft frequency

References

[1] W. Wang, Y. P. Li, M. K. Osman, S. Q. Yuan, B. Y. Zhang and J. Liu, Multi-condition optimization of cavitation performance on a double-suction centrifugal pump based on ANN and NSGA-II, *Processes*, 8 (9) (2020) 1124.

[2] Q. R. Si, S. Q. Yuan, J. P. Yuan, C. Wang and W. G, Lu, Multiobjective optimization of low-specific-speed multistage pumps by using matrix analysis and CFD method, *Journal of Applied Mathematics*, 10 (4) (2013) 136195.

[3] Y. Wang and X. Huo, Multiobjective optimization design and performance prediction of centrifugal pump based on orthogonal test, *Advances in Materials Science and Engineering*, 2018 (2018) 1-10.

[4] L. Zhou, W. Shi and S. Wu, Performance optimization in a centrifugal pump impeller by orthogonal experiment and numerical simulation, *Advances in Mechanical Engineering*, 5 (2013) 385809.

[5] Y. Zhang, S. B. Hu, J. I. Wu, Y. Q. Zhang and L. P. Chen, Multi-objective optimization of double suction centrifugal pump using Kriging metamodels, *Advances in Engineering Software*, 74 (2014) 16-26.

[6] R. Tao, R. Xiao, D. Zhu and F. Wang, Multi-objective optimization of double suction centrifugal pump, *Proceedings of the Institution of Mechanical Engineers, Part C: Journal of Mechanical Engineering Science*, 232 (6) (2018) 1108-1117.

[7] D. Shahram and B. Mohamad, Investigation of an efficient shape optimization procedure for centrifugal pump impeller using eagle strategy algorithm and ANN (case study: slurry flow), *Structural and Multidisciplinary Optimization*, 58 (2018) 459-473.

[8] J. S. Zhou, J. S. Zhang and P. Z. Mao, Performance optimization based on genetic algorithm of double suction centrifugal pump, *Advanced Materials Research*, 468-471 (2012) 2565-2568.

[9] J. Pei, W. Wang, M. K. Osman and X. C. Gan, Multiparameter optimization for the nonlinear performance improvement of centrifugal pumps using a multilayer neural network, *Journal of Mechanical Science and Technology*, 33 (2019) 2681-2691.

[10] L. Zhou, L. Bai, W. Li, W. D. Shi and C. Wang, PIV validation of different turbulence models used for numerical simulation of a centrifugal pump diffuser, *Engineering Computations*, 35 (1) (2018) 2-17.

[11] X. Deng, A mixed zero-equation and one-equation turbulence model in fluid-film thrust bearings, *Journal of Tribology*, 146 (3) (2024) 034101.

[12] H. L. Liu, M. M. Liu, Y. Bai and L. Dong, Effects of mesh style and grid convergence on numerical simulation accuracy of centrifugal pump, *Journal of Central South University*, 22 (1) (2015) 368-376.

[13] A. A. Alubokin, B. Gao, Z. Ning, L. L. Yan, Z. X. Jiang and E. K. Quaye, Numerical simulation of complex flow structures and pressure fluctuation at rotating stall conditions within a centrifugal pump, *Energy Science & Engineering*, 10 (7) (2022) 2146-2169.

[14] G. Yang, X. T. Zhao, D. S. Zhang, L. L. Geng, X. Q. Yang and X. F. Gao, Hydraulic components' matching optimization design and entropy production analysis in a large vertical centrifugal pump, *Journal of Mechanical Science and Technology*, 35 (11) (2021) 5033-5048.

[15] M. D. Mckay, R. J. Beckman and W. J. Conover, A comparison of three methods for selecting values of input variables in the analysis of output from a computer code, *Technometrics*, 42 (1) (2000) 55-61.

[16] A. Zeng, H. Ho and Y. Yu, Prediction of building electricity usage using Gaussian process regression, *Journal of Building Engineering*, 28 (2020) 101054.

[17] J. N. Fuhg, M. Marino and N. Bouklas, Local approximate Gaussian process regression for data-driven constitutive models: development and comparison with neural networks, *Computer Methods in Applied Mechanics and Engineering*, 388 (2022) 114217.

[18] E. Schulz, M. Speekenbrink and A. Krause, A tutorial on Gaussian process regression: Modelling, exploring, and exploiting functions, *Journal of Mathematical Psychology*, 85 (2018) 1-16.

[19] S. Petchrompo, D. W. Coit, A. Brintrup, A. Wannakrairot and A. K. Parlikad, A review of Pareto pruning methods for multi-objective optimization, *Computers & Industrial Engineering*, 167 (2022) 108022.

[20] Y. F. Cui, Z. Q. Geng, Q. X. Zhu and Y. M. Han, Review: multi-objective optimization methods and application in energy saving, *Energy*, 125 (2017) 681-704.

[21] T. X. Wu, D. H. Wu, Y. Ren, Y. Song, Y. Q. Gu and J. G. Mou, Multi-objective optimization on diffuser of multistage centrifugal pump base on ANN‐GA, *Structural and Multidisciplinary Optimization*, 65 (2022) 182.

[22] B. Ghadimi, A. Nejat, S. A. Nourbakhsh and N. Naderi, Multi-objective genetic algorithm assisted by an artificial neural network metamodel for shape optimization of a centrifugal blood pump, *Artificial Organs*, 43 (5) (2019) 76-93.

[23] S. Verma, M. Pant and V. Snasel, A comprehensive review on NSGA-II for multi-objective combinatorial optimization problems, *IEEE Access*, 9 (2021) 57757-57791.

[24] S. Chakraborty, TOPSIS and modified TOPSIS: A comparative analysis, *Decision Analytics Journal*, 2 (2022) 100021.
[25] M. H. Ahmadi, H. Hosseinzade, H. Sayyaadi, A. H. Mohammadi and F. Kimiaghalam, Application of the multi-objective optimization method for designing a powered stirling heat engine: Design with maximized power, thermal efficiency and minimized pressure loss, *Renewable Energy*, 60 (2013) 313-322.
[26] F. Zhang, D. Appiah, F. Hong, J. F. Zhang, S. Q. Yuan, K. A. Adu-Poku and X. Y. Wei, Energy loss evaluation in a side channel pump under different wrapping angles using entropy production method, *International Communications in Heat and Mass Transfer*, 113 (2020) 104526.
[27] D. H. Wu, Z. B. Zhu, Y. Ren, Y. Q. Gu and P. J. Zhou, Influence of blade profile on energy loss of sewage selfpriming pump, *Journal of the Brazilian Society of Mechanical Sciences and Engineering*, 41 (10) (2019) 470.
[28] H. C. Hou, Y. X. Zhang, X. Zhou, Z. T. Zuo and H. S. Chen, Optimal hydraulic design of an ultra-low specific speed centrifugal pump based on the local entropy production theory, *Proceedings of the Institution of Mechanical Engineers, Part A: Journal of Power and Energy*, 233 (6) (2019) 715-726.
[29] H. Y. Guan, W Jiang, J. G. Yang, Y. C. Wang, X. H. Zhao, and J. X. Wang, Energy loss analysis of the double-suction centrifugal pump under different flow rates based on entropy production theory, *Proceedings of the Institution of Mechanical Engineers, Part C: Journal of Mechanical Engineering Science*, 234 (20) (2020) 4009-4023.
[30] T. X. Wu, D. H. Wu, S. Y. Gao, Y. Song, Y. Ren and J. G. Mou, Multi-objective optimization and loss analysis of multi-stage centrifugal pumps, *Energy*, 284 (2023) 128638.

Yu Song is a postgraduate of the College of Metrology and Measurement Engineering, China Jiliang University and Zhejiang Engineering Research Center of Fluid Equipment and Measurement and Control Technology. His research interests include intelligent multi-objective optimization of centrifugal pumps.

Denghao Wu, Ph.D, is a Professor. He is the Head Deputy Director of Zhejiang Research Center of Intelligent Fluid Equipment and Digital Measurement and Control Technology at the College of Metrology and Measurement Engineering, China Jiliang University. He has been engaged in teaching and conducted research on control and detection of fluid machinery, optimal design of fluid machinery, and fault diagnosis and analysis of fluid machinery.